Automatic Shape-Based Sorting of Ceramics Using a Robotic Arm with a Vision System

Benchalak Muangmeesri
Industrial Management Engineering Department, Suan Sunandha Rajabhat University, Thailand
benchalak.mu@ssru.ac.th

Sasithorn Khonthon
Industrial Product Design Department, Phranakhon Rajabhat University, Thailand
sasithorn@pnru.ac.th (corresponding author)

Dechrit Maneetham
Mechatronics Engineering Department, Rajamangala University of Technology Thanyaburi, Thailand
dechrit_m@rmutt.ac.th

Received: 15 March 2026 | Revised: 5 April 2026, 18 April 2026, 20 April 2026, and 23 April 2026 | Accepted: 30 April 2026

Licensed under a CC-BY 4.0 license | Copyright (c) by the authors | *DOI: https://doi.org/10.48084/etasr.18759*

ABSTRACT

This study applies robotics arm and vision system technology as a visual system for ceramic product inspection using modern cameras. The system reduces employee inspection errors and expedites the inspection process caused by the differences in the quality of the workpieces. There is a negligible difference between NG and OK workpieces, making visual inspection difficult. Additionally, the error rate increases when employees visually assess the products, increasing inspection expenses. Ceramic products are classified into five categories: Small, Medium, Large, Covered, and Wide. This study proposes a 5-Degree-of-Freedom (5-DOF) robotic arm with a machine vision system incorporated for an autonomous shape-based ceramic sorting system. For training and validation, a dataset of seventy ceramic objects, bowls, plates, and cups was utilized. Pick-and-place tasks are carried out by the robotic manipulator using the categorization output. The experimental results demonstrate that the system achieves 90% classification accuracy and a sorting speed of 10 pieces per min, indicating an 80% increase in efficiency over human sorting. The proposed approach enables the adoption of smart manufacturing in the ceramic industry and improves production reliability.

Keywords-ceramics; materials; industrial robotics; vision system

I. INTRODUCTION

The Thai government recognizes the ceramics industry as an important sector of the national economy and provides support for its development. The ceramics industry is a significant business connected to other industries, including the building and electrical sectors. This research develops and experimentally evaluates a vision-guided robotic system for automatic shape-based ceramic sorting to lower manual classification mistakes and increase production efficiency in ceramic manufacturing.

A small-scale ceramics production facility involves five key steps: preparation of the clay body, forming, biscuit firing, decorating, glazing and firing, packaging, and distribution. The preparation of clay and the selection of appropriate clay body compositions are considered the most important initial phases in the entire ceramic production process. This is because the type and amount of raw materials used in the clay body during the forming process frequently cause cracking, warping, or other flaws in ceramic products.

Furthermore, clay body shrinkage behavior is a key factor in determining the quality of the final product, and it is highly influenced by the clay composition. Figure 1 shows the raw clay used in a ceramic manufacturing facility. In the early phases of biscuit firing, high shrinkage rates may result in internal tensions, deformation, or cracking, which are undesired effects [1]. Ceramic production uses different forms of clay throughout the workflow, from raw preparation to finished products. Each type serves a different function in forming, supporting, firing, testing, or decorating ceramic ware. Understanding these clay pieces helps ceramists optimize forming processes, reduce defects, and improve overall product quality. In general, clay pieces have the following characteristics: 1) high moisture content, 2) sticky and plastic behavior, and 3) the presence of impurities such as sand, iron spots, organic matter, and other materials.

The rapid development of automation and intelligent manufacturing technologies has significantly transformed the ceramics industry, particularly in processes requiring high precision, repeatability, and rapid classification of workpieces. Traditional ceramic sorting, which relies heavily on manual inspection, is often inconsistent due to operator fatigue, subjective judgment, and environmental variability. These limitations directly impact product quality, production efficiency, and the overall stability of the manufacturing workflow [2, 3]. As consumer expectations rise and production demands intensify, there is a strong need for automated systems capable of performing accurate, high-speed classification of ceramic components based on shape, dimension, and surface characteristics.

Fig. 1. Raw material (clay).

Fig. 2. Roller jigger.

To address these challenges, automatic shape-based sorting systems integrating robotic manipulators and machine vision are promising solutions. In such systems, a camera captures real-time images of ceramic cups or other products moving on a conveyor belt. Through image processing, the machine vision system identifies object boundaries, classifies shapes, and determines the position and orientation of each workpiece. The sorting action is then performed by a multi-axis robotic arm that picks and places the ceramic pieces into designated locations based on the inspection results. This coordinated approach eliminates human error, enhances accuracy, and ensures consistent throughput in fast-paced production environments.

Overall, the proposed system introduces a novel integration of robotic automation, machine vision, and kinematic modeling specifically tailored for the ceramic manufacturing industry, a domain traditionally dominated by manual labor and subjective visual inspection. The novelty of this study lies in its application to delicate ceramic goods and fragile porcelain bowls, which need to be handled carefully to prevent breakage, in contrast to most robotic sorting systems, which focus on stiff and durable industrial parts. To reduce mechanical stress, the proposed method combines controlled robotic manipulation with vision-based inspection.

II. INFLUENCE OF HEAT ON RAW MATERIALS

The many soils, rocks, and minerals that form clay and glaze require firing to achieve the desired material properties. Thus, it is crucial to understand how these materials change their properties as they are fired at increasingly higher temperatures. The investigation of such transformations is based on [4, 5]. These transformations include both chemical and physical.

A. Physical Change

The change in size can be measured in both length and volume. A simple traditional method is to make a test plate, measure its initial length, and then fire it at various temperatures. After the test plate has cooled, its length is measured again at each firing temperature. The shrinkage can then be calculated as a percentage or represented graphically, as:

$$\text{Shrinkage}(\%) = \frac{L_1 - L_2}{L_1} \quad (1)$$

The change in raw materials related to weight loss after firing occurs because such materials, especially clay, contain moisture before firing. This weight loss can be measured using a high-sensitivity balance:

$$\text{Weight Loss}\ (\%) = \frac{W_1 - W_2}{W_1} \quad (2)$$

The change in the raw material density results from the evaporation of water and gaseous radicals, which generate pores within the structure, decreasing the overall density of the material.

B. Chemical Change

The crystalline structure of raw materials changes when they are exposed to heat. As the temperature increases, the crystal structure of the materials undergoes transformation. These structural changes can be studied and analyzed using X-Ray Diffraction (XRD), which provides information about the crystalline phases and can also identify the types and quantities of the mineral components present in the raw materials [6].

Variations in particle size and morphology of the raw materials after firing can be analyzed using an electron microscope to observe surface structure and microstructural changes.

III. MATERIALS AND METHODS

The integration of machine vision with industrial robotics enables automated systems to perceive, interpret, and act upon real-world objects. This integration transforms a robot from a preprogrammed, fixed-path manipulator into an intelligent system capable of adapting to variations in object shape, position, or orientation. In ceramic manufacturing, variability in product dimensions, glaze thickness, surface reflectivity, and firing-induced deformation makes traditional fixed-position robotic gripping insufficient. Machine vision, particularly when implemented through GigE industrial cameras and NI Vision

Builder, provides accurate, real-time object detection and classification, making it possible for a 5-axis robot to autonomously pick, sort, or reject workpieces [7].

$$P_{target} = [Xrobot, Yrobot, Zrobot + Zoffset] \quad (3)$$

$$\Theta_{target} = \Theta_{camera} + \Theta_{robot\_offset} \quad (4)$$

The study focused on three main objectives:

- To design a machine vision algorithm capable of detecting and locating a cup based on its geometric and visual characteristics.
- To implement a robotic arm system capable of performing pick-and-place operations based on visual feedback.
- To analyze system performance in terms of detection accuracy, positioning precision, and processing time.

A. Industrial Robotics

The Intelitek 5-Axis Industrial Robot, as shown in Figure 3, serves as a bridge between educational training systems and industrial automation technology. It replicates the mechanical and control principles of large-scale robots in a safe, user-friendly platform. Its 5-Degree-of-Freedom (5-DOF) allow users to explore kinematic modeling, motion control, vision-based manipulation, and automation system integration. The present study combines the Intelitek 5-Axis Industrial Robot with the NI Vision Builder to design an intelligent robotic workstation that can detect cups placed on a conveyor, analyze their features using machine vision, and then decide whether each cup meets the quality criteria, such as "OK" or "NG" (Not Good). Based on this decision, a robotic gripper picks and places the cups into designated bins or conveyors for further processing. This integration represents a key step toward Industry 4.0 manufacturing, where human visual inspection is replaced with automated robotic intelligence. [8, 9].

B. Robotic Hardware

1) Robotic Arm

A 5-DOF articulated robotic arm was selected for this study. The robot consisted of aluminum links and high-torque servo motors, capable of performing linear and rotational motion. Each joint was driven by a servo motor controlled through a Beckhoff Programmable Logic Controller (PLC), with joint angles computed using Inverse Kinematics (IK) algorithms [10]. The robot's maximum payload is 1 kg, sufficient for ceramic or plastic cups. The main characteristics of the robotic arm are:

- Range of motion: 0° – 180° for each servo joint
- Positional repeatability: ±0.1 mm
- End-effector speed: 200 mm/s

2) End-Effector (Gripper)

In industrial robotics, an effective design for compact and precise gripping motion involves using a servo motor in combination with a bevel gear mechanism. This arrangement converts the servo motor's rotational motion into synchronized opening and closing of the gripper jaws, allowing for high control accuracy and mechanical advantage in limited spaces [11, 12].

3) Work Platform

The experiments were conducted on a flat conveyor belt (100 mm × 600 mm) powered by a 12 V DC servo motor. The conveyor provided a continuous flow of cups for real-time inspection. Conveyor speed is adjustable between 0.1 m/s and 0.4 m/s. A servo motor-driven gripper using bevel gears offers a compact, efficient, and controllable solution for robotic end-effectors [13]. The servo provides precise motion control, while the bevel gear set efficiently transfers torque at a 90° angle, optimizing space and increasing mechanical advantage. Such designs are especially beneficial in industrial robotics, where high precision, light weight, and smooth operation are required, particularly for cup handling, assembly automation, and quality inspection systems.

Fig. 3. Intelitek 5-axis industrial robot.

C. Kinematic Modeling Using Denavit–Hartenberg (D–H)Parameters

Kinematics is a significant concept in robotics, focusing on the study of motion without considering the forces that cause it. In the context of a robotic manipulator, kinematics deals with the relationship between the joint parameters (angles, displacements) and the position and orientation of the end-effector or tool [14]. It enables engineers to predict how a robot moves in space based on the input to its actuators. Figure 4 illustrates the coordinate system of the robotic arm.

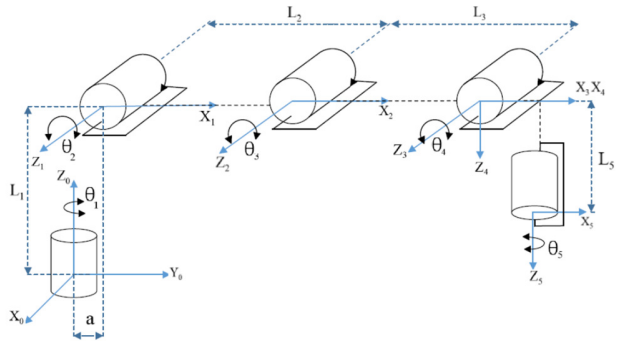

Fig. 4. Coordinate system of the robotic arm.

For an industrial 5-axis robot, which typically possesses 5-DOF, kinematics provides a mathematical framework to control its spatial motion. Such robots are commonly employed in machining, painting, inspection, pick-and-place, and assembly tasks where both position and orientation are important for full five-axis motion. To systematically describe these movements, the D–H parameter convention is employed because it is the most widely used standard in robot modeling and analysis [15, 16]. Table I presents the D–H parameter utilized to describe the motion of the robotic arms.

TABLE I. D–H PARAMETERS

Joint i	$a_i(cm)$	$\alpha_i(rad)$	$d_i(cm)$	$\theta_i(rad)$
1	a = 1.20	$\pi/2$	L_1 =35	θ_1
2	L_2 =22	0	0	θ_2
3	L_3 =22	0	0	θ_3
4	0	$\pi/2$	0	θ_4
5	0	0	L_5 =15	θ_5

For a 5-axis robotic arm, which typically has five joints, the D–H convention helps describe the transformation from the base of the robot to its end-effector through five successive coordinate frames.

$$^{i.1}_{.}T_i = \begin{bmatrix} C\theta_1 & -S\theta_i C\alpha_i & S\theta_i S\alpha_i & a_i C\theta_i \\ S\theta_i & C\theta_i & -C\theta_i S\alpha_i & a_i S\theta_i \\ 0 & S\alpha_i & C\alpha_i & d_i \\ 0 & 0 & 0 & 1 \end{bmatrix} \quad (5)$$

where $\theta_i = sin\theta_i$, $C\theta_i = cos\theta i$, $S\alpha_i = sin\alpha_i$, and $C\alpha_i\, cos\alpha_i$. Each joint and link pair is represented by four D–H parameters: the link length a_i, link twist α_i, link offset d_i, and joint angle θ_i.

$$^{0}_{.}T_1 = \begin{bmatrix} C_1 & 0 & S_1 & aC_1 \\ S_1 & 0 & -C_1 & aS_1 \\ 0 & 1 & C\alpha_i & L_1 \\ 0 & 0 & 0 & 1 \end{bmatrix} \quad (6)$$

$$^{1}_{.}T_2 = \begin{bmatrix} C_2 & -S_2 & 0 & L_2C_2 \\ S_2 & C_2 & -C_1 & L_2S_2 \\ 0 & 0 & 1 & 0 \\ 0 & 0 & 0 & 1 \end{bmatrix} \quad (7)$$

$$^{2}_{.}T_3 = \begin{bmatrix} C_3 & -S_3 & 0 & L_3C_3 \\ S_3 & C_3 & 0 & L_3S_3 \\ 0 & 0 & 1 & 0 \\ 0 & 0 & 0 & 1 \end{bmatrix} \quad (8)$$

$$^{3}_{.}T_4 = \begin{bmatrix} C_4 & 0 & S_4 & 0 \\ S_4 & 0 & -C_4 & 0 \\ 0 & 1 & 0 & 0 \\ 0 & 0 & 0 & 1 \end{bmatrix} \quad (9)$$

$$^{4}_{.}T_5 = \begin{bmatrix} C_5 & -S_5 & 0 & 0 \\ S_5 & C_5 & 0 & 0 \\ 0 & 0 & 1 & L_5 \\ 0 & 0 & 0 & 1 \end{bmatrix} \quad (10)$$

The end-effector transformation matrix $T_0 = {}^{0}_{.}T_5$, is derived by multiplying the five individual transformation matrices defined in (6) – (10) as follows:

$$^{0}_{.}T_5 = {}^{0}_{.}T_1 * {}^{1}_{.}T_2 * {}^{2}_{.}T_3 * {}^{3}_{.}T_4 * {}^{4}_{.}T_5 \quad (11)$$

$$^{0}_{.}T_5 = \begin{bmatrix} K_1 & K_4 & K_7 & p_x \\ K_2 & K_5 & K_8 & p_y \\ K_3 & K_6 & K_9 & p_z \\ 0 & 0 & 0 & 1 \end{bmatrix} \quad (12)$$

The end-effector transformation matrix T_e (also written as ${}^{0}_{.}T_5$) can be computed by substituting these values into (12), which represents the product of all individual homogeneous transformations:

$$\begin{bmatrix} p_x \\ p_y \\ p_z \end{bmatrix} = \begin{bmatrix} 47.3127 \\ 0 \\ 66.1127 \end{bmatrix} \quad (13)$$

D. Inverse Kinematics Structure

IK is the process of determining the joint variables of a robot that achieve a given end-effector pose, consisting of a specific position and orientation:

- Base angle θ_1 determined from (x, y).
- Planar 2-link IK is used to determine θ_2, θ_3 in the vertical plane.
- Wrist angles θ^4, θ_5 obtained from the desired orientation.

With a gripper, the manipulator effectively has three joints for positioning (1–3) and 2 joints for orientation (4–5).

A typical Intelitek SCORBOT-type D-H table has link lengths around:

$d_1 = 0.35$ vertical offset from base to shoulder axis

$a_2 = 0.14$ upper arm length

$a_3 = 0.22$ forearm length

$a_4 = 0.12$ wrist/tool length

The tool pitch (tilt in vertical plane) ϕ is defined as:

$$\phi = \theta_2 + \theta_3 + \theta_4 \quad (14)$$

The IK problem consists of determining $\theta_1, \theta_2, \theta_3, \theta_4$ for a desired TCP pose (x, y, z, ϕ). This is followed by the selection of θ_5.

1. Determination of base joint θ_1

For the base joint θ_1, the horizontal distance from the base axis to TCP is given by:

$$r = \sqrt{x^2 + y^2} \quad (15)$$

Similarly, the base angle is defined as:

$\theta_1 = \text{atan2}(y, x)$

This rotates the arm in the horizontal plane; after that, the analysis is done in a 2D vertical plane at a distance r.

2. Determination of wrist center (x_c, z_c)

To determine the wrist center (x_c, z_c), the base height is removed as:

$z_{rel} = z - d_1 = z - 0.35$

This is followed by the subtraction of the last link a_4 along direction ϕ to get the wrist center (joint 4 position):

$x_c = r - a_4 cos\ \phi = r - 0.12 cos\ \phi$

$z_c = z_{rel} - a_4 sin\ \phi = (z - 0.35) - 0.12 sin\ \phi$ (16)

A 2-link planar problem is obtained with:

Thus, a 2-link planar problem is obtained:

- Link 1: length a_2 =0.14
- Link 2: length a_3 =0.22
- Target point: (x_c, z_c)

Reach distance is defined as:

$distance = \sqrt{x_c^2 + z_c^2}$ (17)

which must satisfy $| a_3 - a_2 | \leq$ dist $\leq a_2 + a_3$ with values:

$| a_3 - a_2 | = | 0.22 - 0.14 | = 0.08$ m and $a_2 + a_3 = 0.14 + 0.22 = 0.36$ m, therefore, $0.08 \leq$ dist ≤ 0.36 for a reachable point.

3. Calculation of elbow angle θ_3

The elbow angle θ_3 is calculated using the cosine law:

$D = \frac{x_c^2 + z_c^2 - a_2^2 - a_3^2}{2 a_2 a_3} = \frac{x_c^2 + z_c^2 - 0.14^2 - 0.22^2}{2 \cdot 0.14 \cdot 0.22}$

If $| D | > 1$, no real solution exists, which indicates a point outside the reachable workspace. Then, the elbow angle is obtained as:

$\theta_3 = \text{atan2}(\pm\sqrt{1 - D^2}, D)$ (18)

where $+$ and $-$ represent the elbow-up and elbow-down configuration, respectively.

4. Determination of shoulder angle θ_2

Shoulder angle θ_2 (angle from shoulder to wrist center) is calculated as:

$\alpha = \text{atan2}(z_c, x_c)$ correction angle for the 2-link geometry:

$\beta = \text{atan2}(a_3 sin\ \theta_3, a_2 + a_3 cos\ \theta_3 = \text{atan2}(0.22 sin\ \theta_3, 0.14 + 0.22 cos\ \theta_3)$

Then: $\theta_2 = \alpha - \beta$ (19)

(using the same sign of θ_3, as in (18))

5. Determination of wrist pitch θ_4

Wrist pitch θ_4 is calculated using the tool pitch relation:

$\phi = \theta_2 + \theta_3 + \theta_4$

Therefore, $\theta_4 = \phi - \theta_2 - \theta_3$ (20)

6. Determination of wrist roll θ_5

Wrist roll θ_5 (roll around the tool axis) only affects orientation, without affecting TCP position, and can be calculated as:

$\theta_5 = \psi$

Selecting a reachable pose for calculation:

Desired TCP:

$x = 0.30$ m

$y = 0.10$ m

$z = 0.40$ m

For the tool pitch $\phi = 0°$(tool horizontal) and tool roll $\psi = 0°$, the base angle is calculated as:

$r = \sqrt{0.30^2 + 0.10^2} = \sqrt{0.09 + 0.01} = \sqrt{0.10} \approx 0.316$ m

$\theta_1 = \text{atan2}(0.10, 0.30) \approx 18.4°8$

Wrist center:

$z_{rel} = z - d_1 = 0.40 - 0.35 = 0.05$ m

$\phi = 0° \Rightarrow cos\ \phi = 1, sin\phi 0$

$x_c = r - 0.12 cos\ 0° = 0.316 - 0.12 = 0.196$ m

$z_c = z_{rel} - 0.12 sin\ 0° = 0.05 - 0 = 0.05$ m

Distance:

distance $= \sqrt{0.196^2 + 0.05^2} \approx \sqrt{0.0384 + 0.0025} \approx \sqrt{0.0409} \approx 0.202$ m, $0.202 \in 0.08, 0.36$

Elbow angle θ_3 is calculated as:

$D = \frac{0.0409 - 0.0196 - 0.0484}{2 \cdot 0.14 \cdot 0.22} = \frac{-0.0271}{0.0616} \approx -0.44 \sqrt{1 - D^2} = \sqrt{1 - 0.44^2} = \sqrt{1 - 0.1936} = \sqrt{0.8064} \approx 0.898$

For elbow-up, $\theta_3 = \text{atan2}(+0.898, -0.44) \approx 116.5°$

Similarly, the shoulder angle θ_2 is calculated as:

$\alpha = \text{atan2}(0.05, 0.196) \approx 14.3°$

$a_3 \sin\theta_3 = 0.22 \cdot 0.898 \approx 0.198$

$a_2 + a_3 \cos\theta_3 = 0.14 + 0.22(-0.44) = 0.14 - 0.0968 = 0.0432$

$\beta = \text{atan2}(0.198, 0.0432 \approx 77.6°)$

$\theta_2 = \alpha - \beta \approx 14.3° - 77.6° = -63.3°$

11. Wrist pitch θ_4:

$\theta_4 = \phi - \theta_2 - \theta_3 = 0° - (-63.3°) - 116.5° = 63.3° - 116.5° = -53.2°$

The wrist roll θ_5 is given by:

$\theta_5 = \psi = 0°$

Final IK angles for this pose

For the Intelitek-type 5-axis arm with link values

$(d_1, a_2, a_3, a_4) = (0.35, 0.14, 0.22, 0.12)$

and desired pose $(x, y, z, \phi) = (0.30, 0.10, 0.40, 0^0)$

$\theta_1 \approx +18.4°$

$\theta_2 \approx -63.3^\circ$

$\theta_3 \approx +116.5^\circ$

$\theta_4 \approx -53.2^\circ$

$\theta_5 \approx 0^\circ$

E. Machine Vision

GigE cameras are a highly reliable and cost-effective imaging technology for industrial recognition tasks, especially when integrated with NI Vision Builder, PLCs, and robotic systems. These advantages make them ideal for ceramic inspection, sorting, object measurement, and robotic guidance. They provide the flexibility of long-distance cabling, high-resolution imaging, multi-camera synchronization, and excellent software compatibility. [17, 18].

F. Covered Ceramic Process Using Machine Vision

The manufacturing process of ceramics involves transforming raw minerals into solid, durable, and sometimes glazed products through a series of physical and chemical changes, including shaping, drying, firing, glazing, and final inspection [19, 20]. Figure 5 shows the traditional ceramic products. The basic ingredients typically used in ceramic manufacturing are presented in Table II.

Fig. 5. Traditional ceramic products.

TABLE II. RAW MATERIAL USED IN CERAMIC PRODUCTION

Raw material	Chemical composition	Function in the ceramic body
Kaolin	Al2O3 .2SiO2.2H2O	This compound is often referred to as China clay
Ball clay	Al2Si2 O5(OH4)	Firing over a higher temperature range
Feldspar	K2O Al2O3 6SiO2	Enabling the clay body to lower firing temperatures
Quartz	SiO2	Provides strength, rigidity, and reduces shrinkage
Alumina	Al2O3	Enabling forming processes such as casting or pressing

G. Software Development

The integration of Backhoff PLCs with EtherCAT-based industrial communication and machine vision systems represents a significant advancement in intelligent automation. In modern manufacturing, precision, speed, and quality assurance are crucial, especially in applications such as ceramic cup inspection, object sorting, and automated packaging.

A 5-axis robotic manipulator provides the flexibility to perform complex motion sequences and handle objects with precise orientation. When combined with machine vision, the robot can recognize, classify, and manipulate objects autonomously based on visual feedback [21, 22].

Cameras are necessary for robotic systems because they give robots the ability to perceive their surroundings, adapt, and make decisions. This allows robots to function beyond predetermined motions and achieve intelligent, flexible, and autonomous operation, which is important in contemporary industrial applications like smart manufacturing and ceramic production systems. Figure 6 displays the Personal Computer (PC) and PLC-based control and machine vision system.

(a)

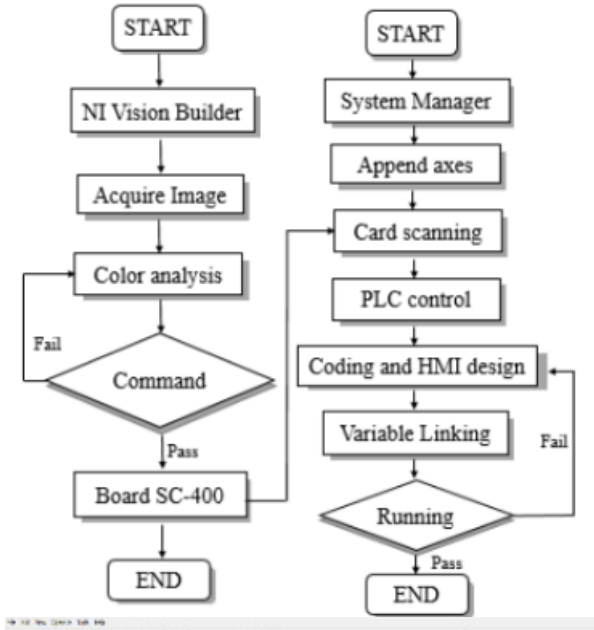

(b)

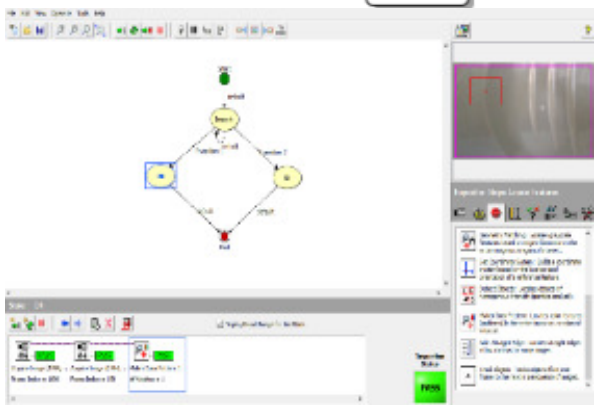

Fig. 6. PC and PLC-based control and machine vision system: (a) flowchart diagram, (b) PLC control of robotics platform.

H. Vision and Integration

Innovation in the ceramic industry has historically progressed slowly compared to other manufacturing sectors such as automotive, electronics, and metal fabrication. The primary reason is the sensitivity and fragility of ceramic ware, which complicates the adoption of automation technologies. Despite advancements in robotics and machine vision across various industries, their integration into ceramic production,

particularly in the sorting, inspection, and handling phases, remains limited. Ceramic products, especially those in the greenware, biscuit-fired, or glaze-fired stages, require very delicate handling. Table III presents the specifications of the camera used in the study.

TABLE III. CAMERA SPECIFICATIONS

Items	Specification and series
Camera	KCMV-SUA502C-T1V
Resolution	2592 × 1944
Frame rate	59 FPS
Sensor size	1/2.5 inch
Pixel size	2.2 μm
Min exposure	0.0084 ms
Shutter type	Rolling shutter
Interface	USB3.0

IV. EXPERIMENTAL RESULTS

In modern industrial automation, machine vision has become an essential technology for achieving intelligent quality inspection, object detection, and sorting. Among the most versatile vision software environments available, NI Vision Builder for Automated Inspection (AI), as shown in Figure 7, developed by National Instruments (NI), allows engineers and researchers to design, test, and deploy vision-based applications without extensive programming knowledge.

(a)

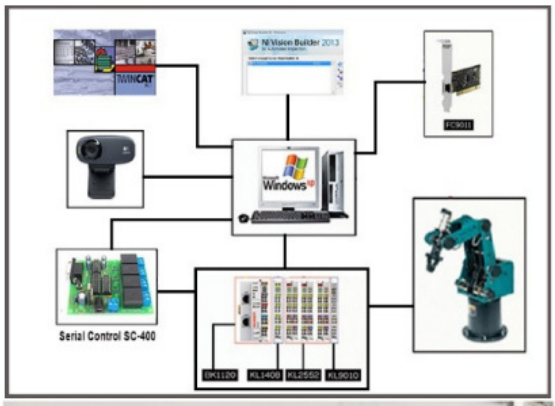

(b)

Fig. 7. Vision technology in ceramic cups: (a) NI Vision Builder, (b) robot and machine vision.

NI Vision Builder can be used to detect and sort cups on a conveyor system based on their position or distance from the camera. The system integrates four main components: a PC running NI Vision Builder, a PLC for motion and sorting control, an industrial camera for image acquisition, and, optionally, a 5-axis or pick-and-place robot for sorting the detected cups [23].

A. NI Vision Builder Software

The combination of NI Vision Builder software, industrial cameras, PLC control, robotic arms, and belt conveyors enables a fully automated system capable of detecting and sorting cups based on distance, as follows:

- The camera provides visual input.
- The PC with NI Vision Builder performs image analysis and measurement.
- The PLC executes control logic and drives actuators or the robot.
- The robot manipulates objects accurately based on the measured coordinates.

Such systems are ideal for the ceramics, packaging, and electronics industries, where precise distance measurement and sorting are crucial [24]. They also represent a fundamental model for Industry 4.0 smart factories, integrating vision, control, and robotics for intelligent production. Figure 8 depicts the inspection process of the inside and outside of the ceramic cup, while Figures 9-11 illustrate the robotics and vision-based inspection process of the ceramic cup.

B. Gripper and Covered Ceramic Cup Processes

A gripper is a type of end-effector used in robotic systems to grasp, hold, manipulate, and release objects during automated operations. It functions similarly to a human hand, acting as the interface between the robot arm and the object being handled. In ceramic production lines, handling covered ceramic cups requires exceptional delicacy because of their fragility, variable sizes, and smooth glazed surfaces [25, 26]. The integration of machine vision, sensors, and intelligent control enables the system to select and handle cups based on their dimensions and distances. The distance between cups is critical for accurate selection and collision prevention. A stereo vision camera or laser distance sensor measures spacing on the conveyor in real time. The following parameters are continuously updated:

- Cup center-to-center distance (D): Determines when the robot can grip the next cup.
- Height (H): Helps detect whether the lid is properly placed or missing.
- Orientation angle (θ): Ensures that the handle direction or cup tilt is within the gripping range.
- Finally, evaluating load values during a gripper test is significant for determining whether the gripping force applied by the robot is appropriate for cups of different sizes, dimensions, and weights. Ceramic materials are brittle and highly sensitive to excessive or uneven

mechanical pressure, so the gripping force must be optimized to ensure that the robot can securely hold the cup without causing any cracks or slippage. The load value indicates the static or dynamic load detected on the gripper while holding the cup:

$$Load\ (kgf) = \frac{Gripping\ Force\ (N)}{9.81} \quad (21)$$

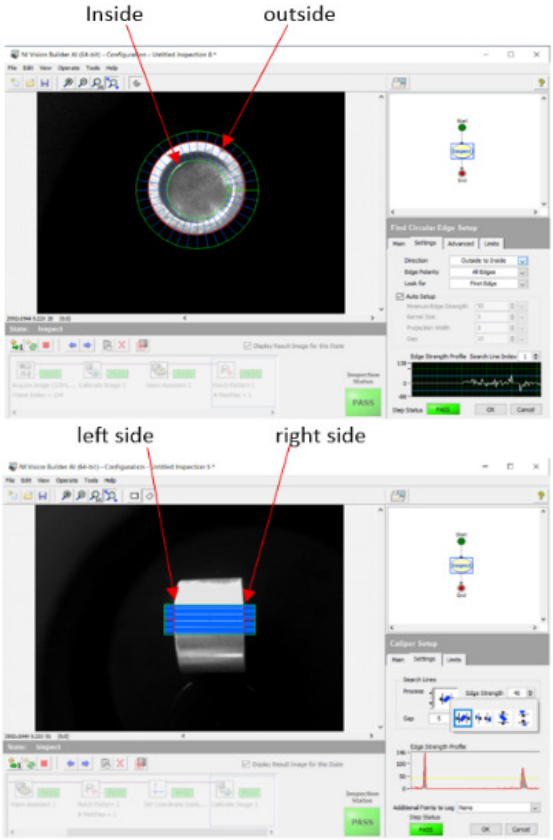

Fig. 8. Inspection of inside and outside of ceramic cup: (a) inside and outside measurement; (b) distance measurement.

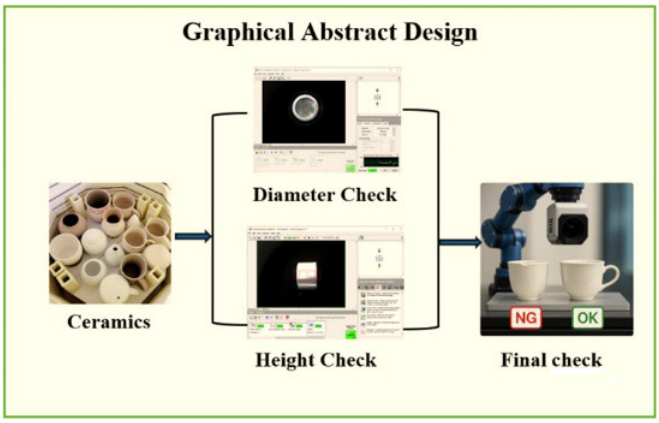

Fig. 9. Robotics and vision-based inspection of a ceramic cup.

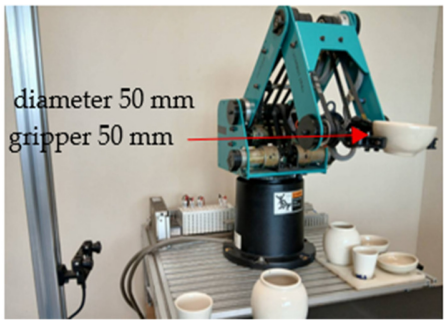

Fig. 10. Inspection and measurement of the cup diameter.

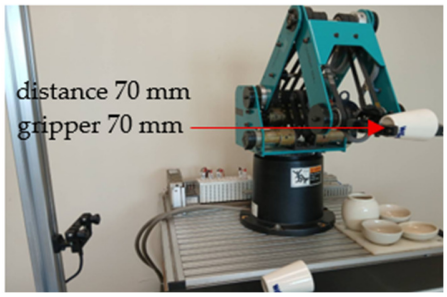

Fig. 11. Inspection and measurement of the cup shape.

TABLE IV. LOAD VALUE EVALUATION

Cup type	Diameter (mm)	Height (mm)	Weight (g)	Gripping force (N)	Load (kgf)
Small	40	60	100	6.2	0.63
Small	45	65	120	6.5	0.66
Medium	50	70	132	6.9	0.70
Medium	55	76	136	7.3	0.74
Large	60	82	143	7.6	0.77
Large	65	86	148	8.1	0.82
Covered	70	90	153	8.7	0.88
Covered	75	93	158	9.2	0.93
Wide	80	98	163	9.8	0.99
Wide	85	102	168	10.4	1.06

As shown in Table IV, there is a positive correlation between the cup diameter and the required gripping load. To evaluate the performance of the automatic shape-based ceramic sorting system, a controlled experiment was conducted using 70 ceramic cups representing five different categories. Classification accuracy indicates how many cups were correctly recognized:

$$\text{Accuracy} = \frac{Number\ of\ Correct\ Classifications}{Total\ Samples} \times 100 \quad (22)$$

Out of 70 cups, the system correctly identified 63. The experiment was expanded by testing an additional 70 ceramic samples to overcome the limitation of the small original sample size. The system achieved a 90% classification accuracy by accurately identifying 63 out of 70 samples. A preliminary evaluation of system performance can be obtained by focusing solely on classification accuracy and sorting seeds.

Using (12), basic performance accuracy is calculated as:

$$\text{Accuracy} = \frac{63}{70} \times 100 = 90\%$$

Mean and standard deviation are calculated using the binomial model, as:

Mean $(\mu) = p = 0.90$ and

Standard deviation$(\sigma) = \sqrt{p(1-p)} = \sqrt{0.90 * 0.10} = 0.30$

This illustrates the variation at the level of individual predictions.

Standard error (SE):

$$\text{SE} = \sqrt{\frac{p(1-p)}{n}} = \sqrt{\frac{0.90*0.10}{70}} \approx 0.0358$$

With confidence interval of 95%.

$\text{CI} = p \pm 1.96 * \text{SE}$

$\text{CI} = 0.90 \pm 1.96 * 0.0358$

$\text{CI} = 0.90 \pm 0.070$

$\text{CI} = (0.83, 0.97)$

$\text{CI} = p \pm 1.96 * SE$ with 95% confidence, the actual system accuracy is probably between 83% and 97%.

TABLE V. LOAD VALUES AND OK/NG CUP DIMENSION

Diameter (mm)	Average load (kgf)	Result
40-55	0.60-0.75	OK
60-75	0.76-0.95	Mixed (OK/NG)
80+	>0.95	Often NG

In this study, the small parallel gripper is mechanically capable of handling ceramic cups with outer diameters up to approximately 80 mm. For larger diameters, secure gripping cannot be guaranteed. Therefore, the proposed vision algorithm is not only responsible for shape-based classification but also measures the outer diameter of each cup and automatically rejects objects larger than 80 mm from the robot's picking list. This integration between vision-based size measurement and gripper capability constraints prevents slipping, collisions, and damage to fragile ceramic workpieces. According to experimental data, the proposed method achieved 90% accuracy under actual production conditions, while human inspection produced an average accuracy of 80%. Additionally, the automated robotic system boosted the sorting throughput from 6 pieces per min (manual) to 10 pieces per min. These findings demonstrate that camera-based separation offers better accuracy, efficiency, and reproducibility.

C. Evaluation of Movement Accuracy and Repeatability

In robotic handling of ceramic cups, especially in processes such as cover placement, glazing, and inspection, the positional accuracy and repeatability of the robotic arm are crucial. Therefore, an experimental study was conducted on the accuracy of movement of a 5-axis robotic arm, focusing on how precisely the robot could move, grip, and place cups of various diameters during the gripper and covered ceramic cup process. This test ensures that each axis of rotational motion and translational motion is correctly synchronized, enabling the gripper to position itself within tight tolerances (±0.1–0.5 mm) without damaging fragile ceramic materials. Table VI presents a description of the 5-axis movement.

TABLE VI. DESCRIPTION OF THE 5-AXIS MOVEMENT

Axis	Joint type	Motion function	Error (mm)
J1	Rotation base	Rotates horizontally across the conveyor	±0.314
J2	Shoulder joint	Moves the arm up/down vertically	±0.215
J3	Elbow joint	Extends/retracts arm reach	±0.382
J4	Wrist pitch	Tilts gripper toward cup surface	±0.722
J5	Wrist rotation	Rotates the gripper about its longitudinal axis	±0.883

To ensure reliable automation in the covered ceramic cup process, a 5-axis error test was performed on the robotic arm, as displayed in Figures 12-16.

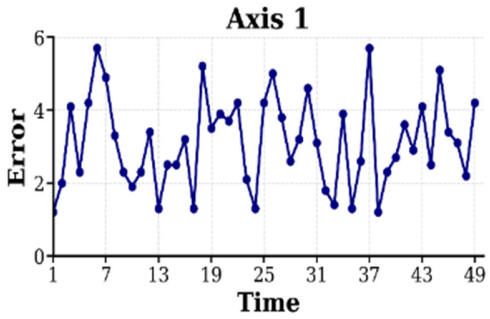

Fig. 12. Axis 1 error test.

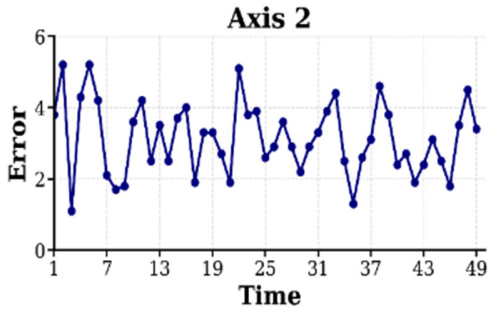

Fig. 13. Axis 2 error test.

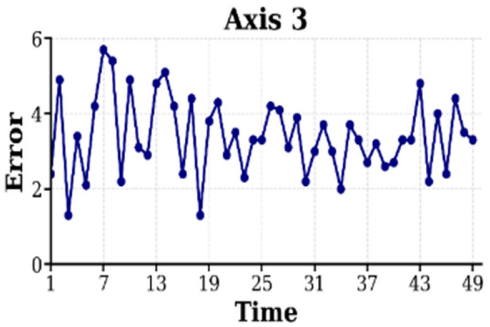

Fig. 14. Axis 3 error test.

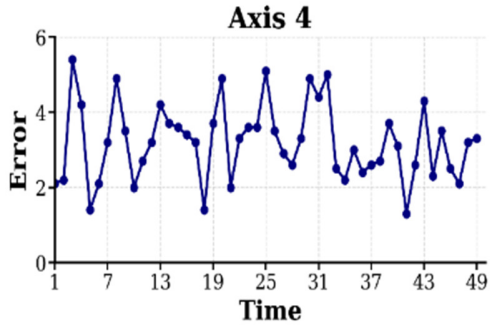

Fig. 15. Axis 4 error test.

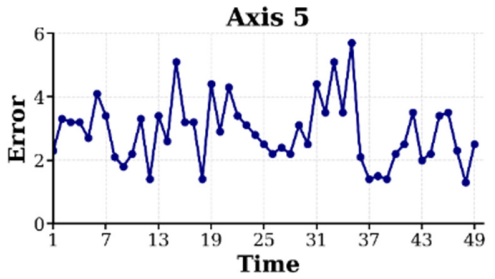

Fig. 16. Axis 5 error test.

V. CONCLUSION

The study examined the Automatic Shape-Based Object Sorting system using a robotic arm integrated with a vision system. This study is organized around the three methods: 1) kinematic modeling using Denavit–Hartenberg (D–H) parameters, 2) machine vision for shape-based recognition, and 3) software development and system integration. The system combines robotic precision with image-processing accuracy to perform sorting based on object shape, dimension, and surface characteristics.

The findings confirmed that the vision-guided robotic arm can identify, classify, and manipulate various ceramic shapes such as cups, plates, and bowls with a high degree of reliability. The vision system, using the NI Vision Builder software and a GigE industrial camera, processed real-time images to detect contours, measure diameters, and distinguish between acceptable (OK) and defective (NG) items. These results were transmitted to the robotic controller, where the 5-axis robotic arm executed corresponding sorting or placement actions. A 5-axis error test of the robotic arm used was also conducted. The measured errors were ±0.314 mm for axis 1, ±0.215 mm for axis 2, ±0.382 mm for axis 3, ±0.722 mm for axis 4, and ±0.883 mm for axis 5.

Overall, the accuracy tests of both the vision detection and robotic motion revealed that the system achieved over 90% classification accuracy and ±0.4 mm positional repeatability under normal operating conditions. The use of machine vision with NI Vision Builder provides a powerful platform for high-resolution imaging, real-time object detection, and robust sorting of ceramic products. This study provides a necessary theoretical and methodological foundation for implementing recognition-based sorting systems in industrial environments and contributes to the advancement of automated ceramic manufacturing processes.

This work improves automated sorting systems by addressing the drawbacks of existing techniques when applied to fragile ceramic objects. Although previous studies have successfully used robotic and vision-based sorting for stiff industrial products, their applicability to ceramics is currently restricted due to problems including surface variations and breakage risk. This work provides a novel integration of a robotic arm and vision system for shape-based ceramic object classification. Unlike previous studies, the proposed approach incorporates a nondestructive handling mechanism and evaluates performance using a larger dataset of 70 samples [27]. With a 90% classification accuracy, the system proved to be viable for real-world industrial applications. Thus, this study extends current understanding by providing a practical and scalable method for automated ceramic sorting. Most studies focus on metals, plastics, or everyday items rather than delicate ceramics; the present study addresses this gap with the following contributions:

- Addressing fragility and handling challenges
- Designing safe gripping and sorting strategies
- Demonstrating real industrial feasibility

The novelty of this study lies in the robotic arm and a shape-based vision algorithm for handling delicate ceramics, which has not been extensively used in ceramic production due to material sensitivity. Additionally, compared with previous studies, the system's high classification accuracy and real-time operational capability make it suitable for industrial implementation.

DECLARATION OF COMPETING INTERESTS

The authors declare no competing interests.

ACKNOWLEDGEMENTS

The authors sincerely acknowledge the support provided for data collection and experimental validation of the robotic sorting system. Special appreciation is extended to the engineers and staff of the PK Ceramics Company, Lampang Province, Thailand, for their valuable assistance and cooperation throughout this study.

DATA AVAILABILITY

The dataset supporting the findings of this study is publicly available at [27].

REFERENCES

[1] A. Quinn, The Ceramics Design Course: Principles, Practice, Techniques. London, UK: Thames & Hudson, 2007.

[2] D. Rhodes, *Stoneware and Porcelain: The Art of High Fired Pottery*. Philadelphia, PA, USA: Literary Licensing, LLC, 2012.

[3] M. Alvarez, L. Brancalião, J. Carneiro, P. Costa, J. P. Coelho, and J. Gonçalves, "Automated Ceramics Tableware Finishing: Non-Circular Geometries Case Study," in *IEEE 28th International Conference on Emerging Technologies and Factory Automation*, Sinaia, Romania, Sep. 2023, pp. 1–6, https://doi.org/10.1109/ETFA54631.2023.10275534.

[4] F. H. Norton, *Elements of Ceramics*. Boston, MA, USA: Addison-Wesley Press, 1952.

[5] X. Liu *et al.*, "Novel Ceramic Clay Automatic Feeding System and Simulation Analysis," *Ceramics*, vol. 7, no. 4, pp. 1413–1439, Oct. 2024, https://doi.org/10.3390/ceramics7040092.

[6] S. Somiya, Ed., *Advanced Technical Ceramics*. Tokyo, Japan: Elsevier Applied Science, 1984.

[7] A. Khan, C. Mineo, G. Dobie, C. Macleod, and G. Pierce, "Vision Guided Robotic Inspection for Parts in Manufacturing and Remanufacturing Industry," *Journal of Remanufacturing*, vol. 11, no. 1, pp. 49–70, Apr. 2021, https://doi.org/10.1007/s13243-020-00091-x.

[8] D. Wang, B. Lutz, P. J. Cobb, and P. Dames, "RASCAL: Robotic Arm for Sherds and Ceramics Automated Locomotion," in *IEEE International Conference on Robotics and Automation*, Xi'an, China, May 2021, pp. 6378–6384, https://doi.org/10.1109/ICRA48506.2021.9561057.

[9] S. Singh, "Machine Vision System for Automated Visual Inspection of Tile's Surface Quality," *IOSR Journal of Engineering*, vol. 2, no. 3, pp. 429–432, Mar. 2012, https://doi.org/10.9790/3021-0203429432.

[10] J. Hernandez *et al.*, "Current Designs of Robotic Arm Grippers: A Comprehensive Systematic Review," *Robotics*, vol. 12, no. 1, Jan. 2023, Art. no. 5, https://doi.org/10.3390/robotics12010005.

[11] Y. Zhang and Z. Wang, "Review of Robotic Grippers for High-Speed Handling of Fragile Foods," *Advanced Robotics*, vol. 39, no. 17, pp. 1054–1070, Sep. 2025, https://doi.org/10.1080/01691864.2025.2508785.

[12] C. I. Rizescu and D. Rizescu, "Gripper for Manipulating Empty Bag Sacks," in *International Conference on Reliable Systems Engineering*, vol. 762, D. D. Cioboată, Ed. Cham: Springer Nature Switzerland, 2023, pp. 418–425.

[13] Z. Ali *et al.*, "Design and Development of a Low-Cost 5-DOF Robotic Arm for Lightweight Material Handling and Sorting Applications: A Case Study for Small Manufacturing Industries of Pakistan," *Results in Engineering*, vol. 19, Sep. 2023, Art. no. 101315, https://doi.org/10.1016/j.rineng.2023.101315.

[14] S. Karupusamy, S. Maruthachalam, and B. Veerasamy, "Kinematic Modeling and Performance Analysis of a 5-DoF Robot for Welding Applications," *Machines*, vol. 12, no. 6, Jun. 2024, Art. no. 378, https://doi.org/10.3390/machines12060378.

[15] D. Gurjeet Singh and V. K. Banga, "Kinematics and Trajectory Planning Analysis Based on Hybrid Optimization Algorithms for an Industrial Robotic Manipulators." In Review, Feb. 02, 2022, https://doi.org/10.21203/rs.3.rs-1313895/v1.

[16] L. Villaverde, D. Maneetham, and P. N. Crisnapati, "Predictive Maintenance Algorithm of a 6-DOF Robotic Arm using Gradient Boosting Regression," *Engineering, Technology & Applied Science Research*, vol. 15, no. 1, pp. 19091–19098, Feb. 2025, https://doi.org/10.48084/etasr.9146.

[17] E. A. Rodríguez-Martínez, W. Flores-Fuentes, F. Achakir, O. Sergiyenko, and F. N. Murrieta-Rico, "Vision-Based Navigation and Perception for Autonomous Robots: Sensors, SLAM, Control Strategies, and Cross-Domain Applications—A Review," *Eng*, vol. 6, no. 7, Jul. 2025, Art. no. 153, https://doi.org/10.3390/eng6070153.

[18] H. Sekkat, S. Tigani, R. Saadane, and A. Chehri, "Vision-Based Robotic Arm Control Algorithm Using Deep Reinforcement Learning for Autonomous Objects Grasping," *Applied Sciences*, vol. 11, no. 17, Aug. 2021, Art. no. 7917, https://doi.org/10.3390/app11177917.

[19] W. D. Kingery, *Introduction to Ceramics*, 2nd ed. New York City, NY, USA: John Wiley & Sons, 1991.

[20] M. Wildenhain, *Pottery: Form and Expression*. New York City, NY, USA: Reinhold Publishing Corporation, 1959.

[21] C. D. Vo, D. A. Dang, and P. H. Le, "Development of Multi-Robotic Arm System for Sorting System Using Computer Vision," *Journal of Robotics and Control*, vol. 3, no. 5, pp. 690–698, Sep. 2022, https://doi.org/10.18196/jrc.v3i5.15661.

[22] K. Wang, Z. Li, and X. Wang, "Concatenated Network Fusion Algorithm (CNFA) Based on Deep Learning: Improving the Detection Accuracy of Surface Defects for Ceramic Tile," *Applied Sciences*, vol. 12, no. 3, Jan. 2022, Art. no. 1249, https://doi.org/10.3390/app12031249.

[23] C.-Y. Cheng, J.-C. Renn, I. Saputra, and C.-E. Shi, "Smart Grasping of a Soft Robotic Gripper Using NI Vision Builder Automated Inspection Based on LabVIEW Program," *International Journal of Mechanical Engineering and Robotics Research*, pp. 737–744, 2022, https://doi.org/10.18178/ijmerr.11.10.737-744.

[24] D. Jancarczyk, J. Rysiński, and J. Worek, "Comparative Analysis of Measurement Tools in the Cognex D900 Vision System," *Applied Sciences*, vol. 14, no. 18, Sep. 2024, Art. no. 8296, https://doi.org/10.3390/app14188296.

[25] M. Kang, S. Yoon, and T. Kim, "Computer Vision-Based Adhesion Quality Inspection Model for Exterior Insulation and Finishing System," *Applied Sciences*, vol. 15, no. 1, Dec. 2024, Art. no. 125, https://doi.org/10.3390/app15010125.

[26] C. Yang, J. Kim, D. Kang, and D.-S. Eom, "Vision AI System Development for Improved Productivity in Challenging Industrial Environments: A Sustainable and Efficient Approach," *Applied Sciences*, vol. 14, no. 7, Mar. 2024, Art. no. 2750, https://doi.org/10.3390/app14072750.

[27] B. Muangmeesri, S. Khonthon, and D. Maneetham, "Ceramic Cup Dataset." Zenodo, May 16, 2026, https://doi.org/10.5281/ZENODO.20225856.